Giant excitonic absorption and emission in two-dimensional group-III nitrides

Maria Stella Prete, Davide Grassano, Olivia Pulci, Ihor Kupchak, Valerio Olevano, Friedhelm Bechstedt

SCIENTIFIC REPORTS
nature research

Check for updates

OPEN

Giant excitonic absorption and emission in two-dimensional group-III nitrides

Maria Stella Prete[1], Davide Grassano[1]✉, Olivia Pulci[1], Ihor Kupchak[2], Valerio Olevano[1,3] & Friedhelm Bechstedt[4]

Absorption and emission of pristine-like semiconducting monolayers of BN, AlN, GaN, and InN are systematically studied by ab-initio methods. We calculate the absorption spectra for in-plane and out-of-plane light polarization including quasiparticle and excitonic effects. Chemical trends with the cation of the absorption edge and the exciton binding are discussed in terms of the band structures. Exciton binding energies and localization radii are explained within the Rytova-Keldysh model for excitons in two dimensions. The strong excitonic effects are due to the interplay of low dimensionality, confinement effects, and reduced screening. We find exciton radiative lifetimes ranging from tenths of picoseconds (BN) to tenths of nanoseconds (InN) at room temperature, thus making 2D nitrides, especially InN, promising materials for light-emitting diodes and high-performance solar cells.

Since the discovery of graphene, the research on alternative two-dimensional (2D) materials has gained enormous interest. Silicene, germanene, phosphorene, and transition metal dichalcogenides are just a few examples of classes of novel low-dimensional systems which may serve as building blocks for efficient nanoelectronic and nanooptical devices[1–4]. On the other hand, bulk group-III nitrides such as GaN, AlN and InN are important materials for solid state lighting, as witnessed by the Nobel prize awarded in 2014 to Akasaki, Amano and Nakamura[5]. The possibility to play with dimensionality to enhance the already exceptional properties of bulk nitrides has caused many attempts to grow 2D nitrides, although the strong tendency for sp^3 bonding makes their preparation extremely difficult. Only monolayer BN can, in principle, be easily prepared by exfoliation from hexagonal bulk BN[6]. Promising experimental attempts to obtain 2D AlN and GaN recently appeared[7–9]. Measurements of GaN sheets encapsulated in graphene seem to suggest a fundamental optical gap of about 5 eV[10]. Gaps even larger than in BN have been found for low-dimensional AlN structures[9]. These successful experiments pave the way to new photovoltaic and optical nanodevices based on 2D nitrides[11].

Experimental activities to synthetize monolayer and few-layer group-III nitride sheets are accompanied by theoretical studies. For graphene-like, hexagonal 2D AlN and GaN, their dynamical stability has been explored and verified by phonon or even molecular-dynamics calculations[12–16]. The progress in theoretical growth predictions has been recently summarized in a review paper[11]. Although the crystal structure of freestanding AlN and GaN is under debate, most studies favor a planar, honeycomb structure[11,12,17,18].

The recent progress in achieving growth of ultrathin 2D AlN and GaN layers on substrates, as well as the exfoliation of BN monolayers, suggest the possibility to prepare also 2D InN. Therefore, a theoretical understanding of the monolayer properties of BN, AlN, GaN, and InN, in particular of their electronic structure as well as optical absorption and emission properties, may push forward the experimental activities on 2D nitrides and their possible optoelectronic applications. Several studies have been focused on the tunability of the electronic gap[13–16,19,20]. Excitonic properties have been recently investigated for GaN[15,16,16,21] and InN[22,23], in addition to what was already found on the well-known BN layer ([18,24] and references therein).

In this letter we study the excitons of the 2D group-III nitrides BN, AlN, GaN and InN relying on data from ab initio calculations of the electronic structure and optical properties. We focus on the onset of optical absorption and emission spectra for both in- and out-of-plane light polarization. We study the main bound excitons with regards in particular to the influence of spatial confinement effects and reduced screening of the

[1]Dipartimento di Fisica, Università di Roma Tor Vergata, INFN, Via della Ricerca Scientifica 1, 00133 Rome, Italy. [2]V.E. Lashkaryov Institute of Semiconductor Physics, National Academy of Sciences of Ukraine, Kyiv, Ukraine. [3]CNRS, Institut Neel, 38042 Grenoble, France. [4]IFTO, Friedrich Schiller Universität, Max-Wien Platz 1, 07743 Jena, Germany. ✉email: davide.grassano@roma2.infn.it

electron-hole interaction. For the lowest exciton we calculate the binding energy and the excitonic radius and compare the results with those of model calculations. Finally we determine the excitonic radiative lifetime to characterize the optical emission.

Methods

Structural and electronic properties are calculated from ab initio with a three steps procedure: first, the equilibrium geometry of 2D honeycomb sheets , e.g. the lattice constants and the atomic coordinates, is determined by minimizing the total energy within the density-functional theory (DFT)[25] in the local-density approximation (LDA) using the *Quantum Espresso* code[26,27]. The isolated 2D crystals are modeled by a supercell approach with a vacuum layer of thickness L of about 15 Å between the periodic images. Second, starting from the DFT Kohn–Sham electronic structure we calculate the quasi-particle energies $\varepsilon_{n\mathbf{k}}^{G_0W_o}$ in the G_0W_0 approximation for the self-energy by the *chisig* code[28]. For the exchange part of the self-energy, we use a $102 \times 102 \times 1\,\mathbf{k}$-point mesh centered on Γ in the Brillouin Zone (BZ). For the correlation part of the self-energy and for the screened Coulomb interaction W, we use a $51 \times 51 \times 1\,\mathbf{k}$-point mesh and 300 bands. To avoid interaction between spurious replica of the monolayers, we apply to the Coulomb potential a cut-off at the vacuum layer boundary.

Electron-hole pairs. In the third step, we solve the homogeneous Bethe–Salpeter equation (BSE)[29] in the Tamm–Dancoff approximation by the *dp4exc* code[30]. To account for the electron-hole attraction, the BSE kernel is approximated by an electron-hole static screened interaction term W beyond the electron-hole exchange term v. Electron-hole pair (exciton) states $|S\mathbf{Q}\rangle$ with energies $E_S(\mathbf{Q})$, labeled by the quantum number S and the translation momentum $\hbar\mathbf{Q}$, are the eigenstates of the excitonic Hamiltonian H_{exc} and can be obtained by diagonalizing it. The optical spectra are calculated using a mesh of $51 \times 51 \times 1$ k-points. The number of occupied (empty) bands are 3 (3 for BN, 4 for AlN, 5 for GaN and InN). A cut in the Coulomb potential was applied.

For the lowest-energy, at the onset of the absorption spectrum, ground-state bound excitons $S = 0, \mathbf{Q} = 0$ binding energy E_b and radius r_{exc}, obtained within the accurate, but computationally heavy BSE calculations[31], are compared with predictions of an analytical model of excitons in two dimensions[32,33]. The model Schrödinger equation in (SM1) relies on the effective mass approximation (EMA), with the reduced exciton mass $\mu = m_e m_h/(m_e + m_h)$ in terms of the electron (hole) mass m_e (m_h) extracted from the dispersion of the lowest conduction (highest valence) band. The screened Coulomb interaction between the electron and the hole is described by a Rytova-Keldysh potential[33–35] whose distance dependence is ruled by the 2D static electronic polarizability of the sheet, $\alpha_{2D} = L \cdot (\,\mathrm{R}\, e\epsilon_{\parallel}(\omega = 0) - 1)/4\pi$, which is computed from the in-plane dielectric function $\epsilon_{\parallel}$ in the limit of vanishing wave vector and frequency. The lowest exciton state is determined by a variational approach (see Supplementary Material for more details).

Optical properties. With the eigenstates of the BSE excitonic Hamiltonian $E_S(\mathbf{Q} = 0)$, $|S, \mathbf{Q} = 0\rangle = \sum_{vc\mathbf{k}} A_S^{vc\mathbf{k}} |v\mathbf{k}\rangle |c\mathbf{k}\rangle$ at zero-momentum transfer $\mathbf{Q} = 0$ (the photon wave vector is negligible with respect to crystal momenta), we can calculate the optical conductivity $\sigma_{\parallel/\perp}(\omega)$[36] or equivalently the frequency-dependent dielectric tensor $\epsilon_{\parallel/\perp}(\omega)$ for light polarization parallel/perpendicular to the crystal sheets,

$$\epsilon_{\parallel/\perp}(\omega) = 1 + \frac{4\pi}{AL}\left(\frac{e}{m\omega}\right)^2 \sum_S \frac{|\sum_{vc\mathbf{k}} A_S^{vc\mathbf{k}} \langle c\mathbf{k}|p_{\parallel/\perp}|v\mathbf{k}\rangle|^2}{\hbar\omega - E_S - i\eta}$$

with $\langle c\mathbf{k}|p_{\parallel/\perp}|v\mathbf{k}\rangle$ as optical transition matrix elements between KS valence ($|v\mathbf{k}\rangle$) and conduction ($|c\mathbf{k}\rangle$) states and the unit area A. The imaginary part $\mathrm{Im}\epsilon_{\parallel/\perp}(\omega)$ is related to the optical absorption for in- and out-of-plane light polarization.

Finally, following Ref.[37], we calculate the radiative decay rate $\gamma_S(0)$ and lifetime $\tau_S(0)$ of an exciton in state S with vanishing wavevector $\mathbf{Q} = 0$ as[38]

$$\gamma_S(0) = \tau_S^{-1}(0) = \frac{8\pi e^2 E_S(0)}{\hbar^2 c} \frac{\mu_S^2}{A_{uc}}, \tag{1}$$

where μ_S^2 is the square modulus of the exciton dipole transition matrix element. A_{uc} is the area of the unit cell and $E_S(0)$ is the exciton excitation energy. To compute the thermally averaged radiative lifetimes $\langle\tau_S\rangle$ of excitons in excitonic bands $E_S(\mathbf{Q})$ at temperature T we apply the formula obtained in the classical high-temperature limit[38]

$$\langle\tau_S\rangle = \tau_S(0)\frac{3}{4}\left(\frac{E_S^2(0)}{2Mc^2}\right)^{-1} k_B T \tag{2}$$

with $M = m_e + m_h$ being the translational (total) mass of the exciton.

Results

Geometry and electronic properties. 2D sheets of group-III nitrides have as equilibrium geometry a flat honeycomb structure similar to graphene[39] but with reduced D_{3h} symmetry. As in graphene and BN, also in AlN, GaN and InN the first-row element N tends toward a sp^2 hybridization and in-plane III-N bonds. Therefore, the geometries are only characterized by the lattice constant a. The lattice parameters, listed in Table 1, follow a clear chemical trend with increasing atomic number of the cation. The lattice constants are smaller than those for the 3D bulk counterparts, consistently with the sp^2 bonding being stronger than the sp^3 one.

	a (Å)	E_g (eV)	E_b (eV)	r_{exc} (Å)	α_{2D} (a.u.)	m_h/m_e (m)	$\tau_S(0)$ (fs)	$\langle\tau_S\rangle$(ps)
BN	2.48	7.2 (KK)/6.7 (KΓ)	2.0 (2.1)	3.8 (3.7)	2.10	0.63/0.97	29 (13)	55 (14)
AlN	3.03	6.5 (ΓΓ)/5.8 (KΓ)	1.9 (2.3)	4.5 (3.4)	2.07	1.64/0.59	33 (1)	67 (18)
GaN	3.15	4.5 (ΓΓ)/ 4.6 (KΓ)	1.2 (1.4)	8.0 (6.6)	2.78	0.52/0.26	35 (18)	73 (36)
InN	3.52	1.7 (ΓΓ)/2.1 (KΓ)	0.6 (0.5)	15.5 (16.4)	7.76	0.42/0.09	55 (58)	422 (445)

Table 1. Lattice constant a and direct and indirect QP gaps E_g. The band edge positions in the BZ are indicated in parenthesis. Excitonic binding energy E_b and excitonic radius r_{exc} at the BSE level and, in parenthesis, within the 2D effective Hamiltonian. Also the DFT ingredients α_{2D} and the electron and hole effective masses are reported. Last two columns: calculated exciton radiative lifetimes $\tau_S(0)$ for 2D III-nitrides at zero temperature (Eq. 1) and $\langle\tau_S\rangle$ (Eq. 2) at room temperature for bound excitons in the ground state $S = 0$ and $\mathbf{Q}$=0. The values in parenthesis have been estimated within the effective mass approximation but ab-initio calculated optical matrix elements.

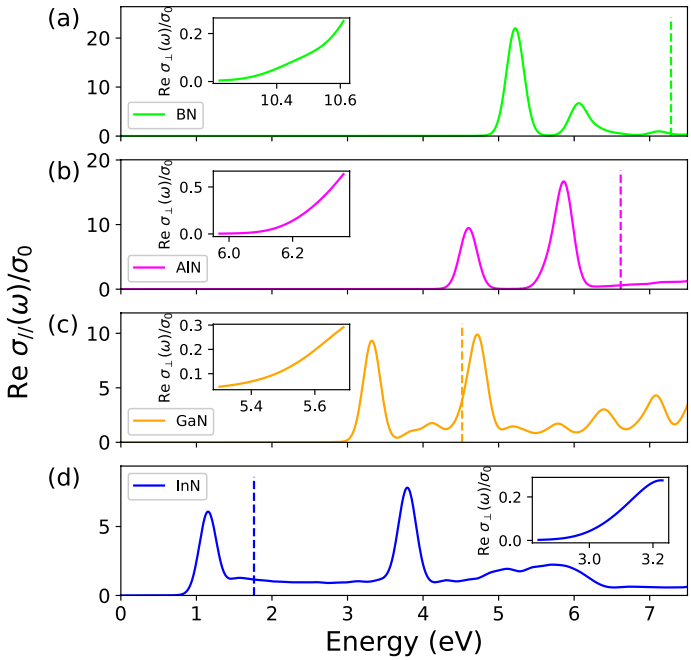

Fig. 1. Real part of the dynamical optical conductivity Re $\sigma_{\parallel}(\omega)$ for in-plane polarization of **(a)** BN, **(b)** AlN, **(c)** GaN and **(d)** InN. The insets show the onset of absorption for out-of-plane polarization. The spectra are normalized to the dc conductivity σ_0. The direct QP gap is indicated by a vertical dashed line.

The electronic properties of the 2D III-N monolayers, conversely to graphene, do not show any Dirac cone in the electronic band structure[16,19,20,39]. The band structures, see Supplemental Material (SM) Fig. SM1, are characterized by indirect gaps with the valence band maximum (VBM) at K and the conduction band minimum (CBM) at Γ. Apart from BN with a pronounced lowest direct band gap at K, the other nitrides exhibit a direct gap at Γ. While BN and AlN tend to be indirect semiconductors, GaN and InN are direct 2D crystals[19]. Table 1 indicates that the valence band maxima at Γ and K are not far away from each other. Consequently, for GaN, the direct and indirect gaps of 4.53 and 4.57 eV are close to each other. Indirect gaps of 4.55 eV[14], 4.38[15] and 4.44 eV[16] have also been computed. Fully self-consistent QP calculations[15] seem to strengthen the tendency for a direct gap at Γ but with a larger value of 5.39 eV. Experimental values of GaN layers embedded in AlN cover a wide range of 4.76–5.44 eV[40] not too far from all the QP gaps. Moreover, the QP gap values in Table 1 are close to those found in the literature for BN[18], AlN[19], GaN[15,16,19,21] and InN[19,20,22].

The gap values E_g, listed in Table 1 are due to VBM composed primarily of N2p_z orbitals, while the CBM is a hybridization of group-III s and some N2s states. The gaps arise from the presence of two different kinds of atoms, bearing different electronegativity, in the two hexagonal sublattices. A charge transfer occurs from the cation (B, Al, Ga, In) to the anion (N) with a subsequent opening of the electronic QP gaps, which span from about 7 eV for 2D BN to 1.7 eV for 2D InN, respecting the chemical trend. The electronic gaps shown by 2D III-N monolayers are much larger than those of their 3D bulk counterparts (see collections in[13,24,41]). Quantum confinement of the electrons is mainly responsible for this behavior. In addition, the reduced 2D screening also modifies the QP corrections.

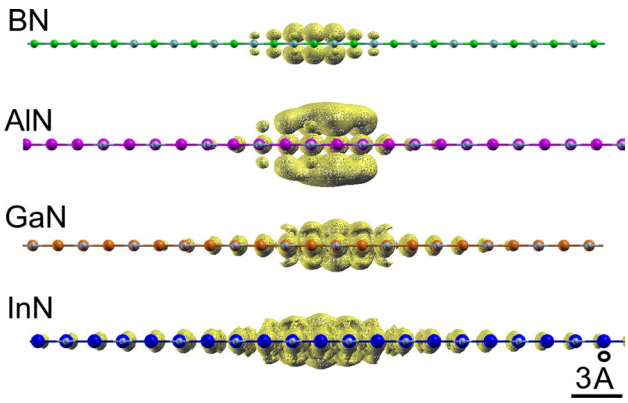

Fig. 2. Exciton wavefunctions for the 2D nitrides. In all cases the hole has been fixed near a nitrogen atom (light blue). (Figure prepared using XCrySDen v1.5.60[49], http://www.xcrysden.org/).

Excitonic effects in optical spectra. The absorption spectra including the QP and excitonic effects are displayed in Fig. 1. Indeed the real part of the optical conductivity represents the absorbance for vanishing reflectance. The inclusion of electron-hole interaction through BSE leads to a redshift of the absorption spectra and seems to compensate the quasiparticle effects, restoring a qualitative agreement with the position of DFT spectra but not their lineshape (see Figs. SM2 to SM5). For in-plane light polarization strong peaks appear due to bound excitons, well below the fundamental direct gaps. For GaN and InN, and especially InN, such bound exciton peaks also occur above the fundamental QP gap belonging to high-energy interband transitions and, hence, being resonant with the continuum of scattering states of higher valence-conduction band pairs. The striking difference between the two light polarizations is the significant blueshift of the absorption spectra Re $\sigma_{\perp}(\omega)$ mainly due to local-field or depolarization effects described by the electron-hole exchange interaction in the two-particle Hamiltonian H_{exc}[18,36,37,42]. Also their intensities are reduced, in particular for BN.

In Fig. 1 we focus on the onset of the absorption spectra for in-plane light polarization. For BN the onset is characterized by three low-energy peaks of decreasing intensity. For the first exciton at 5.2 eV, usually identified as optical gap E_g^{opt} reduced by the binding energy E_b with respect to the QP gap E_g, we find a large exciton binding energy of 2.0 eV. A second and a weak third peak appear at 6.1 eV and 7.2 eV (see Fig. SM2), respectively. The first structure originates from transitions at the fundamental gap at K between the highest valence band and the lowest conduction band. The second exciton peak has a similar origin (see Fig. SM1). The first two band-edge excitons are related to $\pi \rightarrow \pi^*$ transitions. The third peak belongs mainly to transitions near Γ with some hybridization with σ and σ^* states. Although the position of the peaks is slightly different, our value of the binding energy is in agreement with other predictions[18,24,43]. The AlN in-plane conductivity exhibits two prominent structures of increasing intensity, located at 4.6 eV and 5.9 eV. The binding energy of the first exciton is 1.9 eV. In a previous theoretical work[44] three excitons peaks at 4.12 eV, 4.97 eV and 5.4 eV were found with a similar binding energy of 1.88 eV. Also for GaN we register the presence of two main peaks for the in-plane component of the BSE sheet polarizability near the absorption edge. The first peak appears at 3.3 eV while the second is at 4.7 eV (see also SM), similarly to other calculations[16]. The first exciton presents a large binding energy of 1.2 eV in agreement with Refs.[15,16,21]. According to Fig. SM1(c), the first exciton is built by allowed, mainly $\sigma \rightarrow \sigma^{\star}$, optical transitions between the highest two valence bands and the lowest conduction band near Γ. The second broader excitonic feature in Fig. 1 and Fig. SM4(a) with partial resonant character is mainly related to the lowest energy $\pi \rightarrow \pi^{\star}$ transitions near K, combined with transitions along the $K \rightarrow M$ line in the BZ, because of the flatness of the lowest conduction and highest valence bands. However, also contributions between the highest valence bands and the second lowest conduction band near Γ, with $\sigma \rightarrow \pi^{\star}$ character, do contribute. Two bound excitons appear for InN in the BSE optical conductivity for in-plane light polarization below photon energies of 6 eV. The first exciton, at 1.2 eV, has a binding energy of 0.6 eV and originates VBM-CBM transitions near Γ. A second bound but resonant exciton peak, visible at 3.9 eV, arises from valence-conduction band transitions near M and K at the BZ boundary.

Exciton binding and localization. In all 2D nitrides the first strong excitonic peak originates from transitions at the fundamental direct gap between the highest valence band and the lowest conduction band near Γ (K in the BN case). Their binding energies E_b are strongly related to the exciton radii r_{exc} as expressed by the chemical trends in Table 1 and Fig. 3. Thereby, the exciton radius has been derived ab-initio from the expectation value with the computed exciton wavefunctions. The corresponding exciton wave functions are plotted in Fig. 2. They represent the probability to find the electron, having fixed the position of the hole near one nitrogen atom. Their localization around the chosen hole position clearly indicates the 2D character of the excitons, which extend above and below the basal plane just for a length of the order of the lattice parameter. The lateral electron-hole distance covers instead a wider range in Fig. 2. By defining the excitonic radius r_{exc} as the first moment

$$r_{exc} = \int d^3\mathbf{r}_e |\mathbf{r}_e| \psi^*(\mathbf{r}_h, \mathbf{r}_e) \psi(\mathbf{r}_h, \mathbf{r}_e), \tag{3}$$

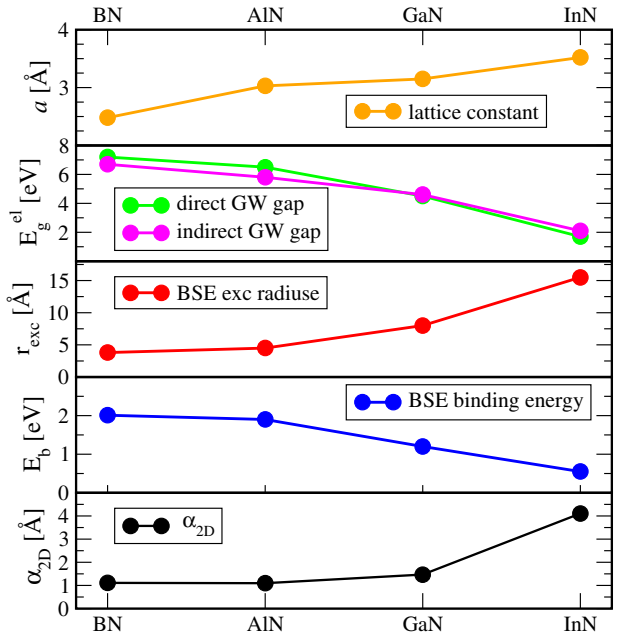

Fig. 3. Ab-initio results for lattice constant, direct and indirect QP gaps, exciton radius, binding energy of the excitons and the 2D static polarizability.

where $\psi(\mathbf{r}_h, \mathbf{r}_e)$ denotes the exciton eigenstate $|S\mathbf{Q}\rangle$ for the state $S = 0$ and $\mathbf{Q} = 0$ in real-space representation, we find an excitonic radius as small as 3.8 Å for 2D BN, and as large as 15.5 Å for 2D InN. Comparing the values r_{exc} with the lattice constants a in Table 1, a clear tendency for the formation of 2D excitons in the ground state from BN to InN becomes visible. The averaged electron-hole distances r_{exc} in BN and AlN are not significantly larger than the lattice parameters. Their lowest energy excitons may be therefore interpreted to possess a Frenkel-like character. Electron and hole in the excitons are found close to nearest-neighbor atoms in the plane with the highest probability. In the case of GaN and InN, however, the larger electron-hole distances r_{exc} suggest a character, which tends to be closer to that of 2D hydrogen-like Wannier–Mott excitons. In any case, the excitonic features in the 2D nitrides are much stronger compared to their 3D counterparts[41], because of two main reasons: the confinement of the motion of electrons and holes in the 2D honeycomb structure and the weak 2D screening of the electron-hole attraction.

The chemical trends of the exciton parameters E_b and r_{exc} are qualitatively in line with the fundamental QP gaps E_g and the lattice constant a (see Table 1). As summarized in Fig. 3, with increasing cation atomic number we find an increasing lattice constant, accompanied by a decrease of the QP gaps. The exciton binding energy E_b qualitatively follows the gap energy, which characterizes the intrinsic screening in the sheet as visible from the polarizability α_{2D}.

Model 2D excitons. Using the polarizability α_{2D} and mass parameters m_e and m_h from Table 1, the variational approach to 2D excitons[33,34] yields model values for E_b and r_{exc} which are also listed in the same table. They are in good agreement with the BSE results. Moreover, we list in Table SM1 the results obtained by solving the model Hamiltonian in the two opposite (Wannier–Mott and logarithmic[34]) approximations. The results clearly demonstrate that neither the logarithmic limit nor, in particular, the unscreened 2D Coulomb potential for the electron-hole attraction[34] are fit to describe the lowest bound for the 2D nitrides. A quantitative relationship between the two exciton parameters can be approximately given by $E_b \sim \hbar^2/(2\mu r_{\mathrm{exc}}^2)$ with μ as the reduced exciton mass. Using in the above relation our BSE results give a prefactor of about 0.27, thereby confirming that the true ab-initio computed excitons are far from a 2D hydrogen-like model, which would suggest a prefactor 1. The variational solution of the 2D model Hamiltonian, instead, gives a prefactor 0.3, in good agreement with the BSE results. Finally, a linear interpolation using the values obtained within the logarithmic limit gives a prefactor of about 0.5. In other words, the intermediate range is realized, i.e., neither the Wannier–Mott nor the logarithmic behavior gives a reasonable description of the screened potential, although in the logarithmic limit the error is smaller. The reliability of the variational solution of the 2D model Hamiltonian, previously tested on graphane, silicane, and germanane in[33], is demonstrated by comparing the ab-initio and 2D model results in Table 1. For both exciton binding energy and exciton radius the chemical trends and the absolute values are in astonishing agreement. The energy deviations are only of the order of 0.1–0.2 eV and the radii differences are of the order or less than 20%. For the strongest bound exciton in BN practically the same values are obtained within ab-initio and model descriptions. The rough description of the lowest exciton as a 2D 1*s* variational state seems hence to cover the correct physics.

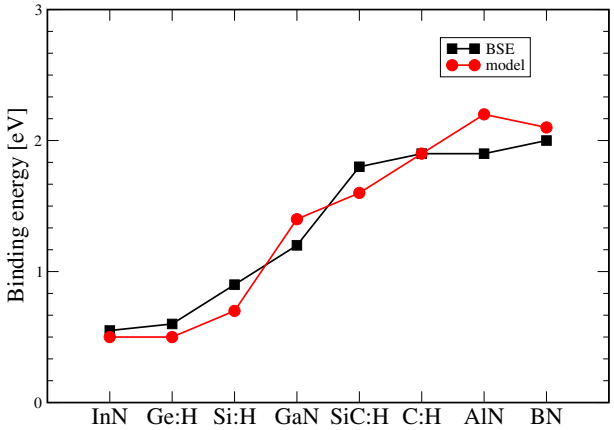

Fig. 4. Comparison of the exciton binding energies calculated ab-initio by solving the BSE (black squares), and by solving the 2D excitonic model (red circles).

Analyzing the variational results in Table 1 we can affirm that the model solutions are in good agreement with the results of full ab-initio but cumbersome BSE calculations. The general validity of this conclusion is underlined in Fig. 4 including the results for the hydrogenated group-IV materials, graphane, silicongraphane, silicane, and germanane[33,45,46], which are in line with the findings for nitride monolayers.

Exciton radiative lifetimes. Important material characteristics for light-emitting diodes and laser devices are the rates of different electron-hole recombination processes. Not much is known at the moment about these processes in 2D nitrides. Here, we focus on the exciton radiative lifetimes and compare the results with the corresponding lifetimes of 3D nitrides. Again, we consider the lowest-energy excitons $S = 0$ and $\mathbf{Q} = 0$ to find the radiative decay time (1) or its thermal average (2). The lifetimes $\tau_S(0)$ of BN, AlN, and GaN are very similar to each other, while for 2D InN it is significantly larger (see Table 1). The lifetimes and the exciton binding energies in Table 1 show opposite trends, in accordance with the Heisenberg uncertainty principle.

The recombination times of the lowest energy excitons, are by more than one order of magnitude smaller than the corresponding lifetimes of excitons of transition metal dichalcogenides at the corner points K of the hexagonal BZ[38]. The main reason for this difference is the stronger transition matrix elements in the case of the nitrides. The radiative lifetimes of the lowest-energy excitons clearly indicate the excellent emission properties of 2D nitrides. They seem to be more appropriate for LED and laser applications than the transition metal dichalcogenides.

The averaged lifetimes for excitons in the lowest-energy exciton band $\langle\tau_S\rangle$ at room temperature still give rise to shorter values than the transition metal dichalcogenides[38]. In general, they possess an averaged radiative lifetime $\langle\tau_S\rangle$, which is three orders of magnitude larger than $\tau_S(0)$. This is a consequence of the much faster recombination of the excitons with vanishing translational energy. Comparing the averaged lifetimes $\langle\tau_S\rangle$ at room temperature in Table 1 with the values for 3D nitrides[47,48], differences of one to two orders of magnitude are observed. This fact, again, underlines the outstanding emission properties of 2D nitrides. Due to the quantum confinement, the reduced screening and, hence, the huge exciton binding energies, the sheet crystals appear as promising materials for active optoelectronic applications.

Finally, for a better understanding of the exciton radiative decay rates, we also apply the variational solutions for the lowest 1s excitons with a pure 2D screening derived in Ref.[33]. With the parameters summarized in Table 1 we find the values given in parenthesis in columns 8 and 9. They are close to those computed ab-initio. These findings indicate that the material dependence, the chemical trend, can be described by $\tau_S(0) \sim E_g^{opt} r_{exc}^2 / |\langle v\mathbf{k}|p_\parallel|c\mathbf{k}\rangle|^2$. For the thermally averaged quantities it holds $\langle\tau_S\rangle \sim \tau_S(0) M/(E_g^{opt})^2$. These relations are in qualitative agreement with the variation of the ab-initio exciton lifetimes with the 2D crystal discussed above. However, Fig. 5 also clearly indicates that the material dependence on the optical matrix element square $|\langle v\mathbf{k}|p_\parallel|c\mathbf{k}\rangle|^2$ is not negligible, at least going from GaN to InN. Along the row BN, AlN and GaN, this dependence is weak. The exciton lifetime $\langle\tau_S\rangle$ at 300 K computed to about 73 (36) ps within the ab-initio (model) scheme for the first exciton in GaN (see also Table 1) has to be related to similarly estimated values of 20 ps[15] or 600 ps[21]. The weak difference in the first case[15] is astonishing because of the used different approaches. The stronger deviation in the second case[21] is probably due to the applied larger exciton mass M estimated by bulk particle values and the different optical transition matrix elements taken into account.

Summary and conclusions

In conclusion, the optoelectronic properties of group-III nitride monolayers have been here investigated ab-initio. The quasiparticle electronic structures are computed within the G_0W_0 approximation. The two-particle excitations and the accompanying optical properties are predicted by solving the Bethe–Salpeter equation with screened electron-hole attraction and unscreened electron-hole exchange. In addition to the absorption of the lowest bound electron-hole pairs, their emission properties are also studied by computing the exciton radiative lifetimes. The characteristic parameters of the bound excitons dominating both absorption and emission have

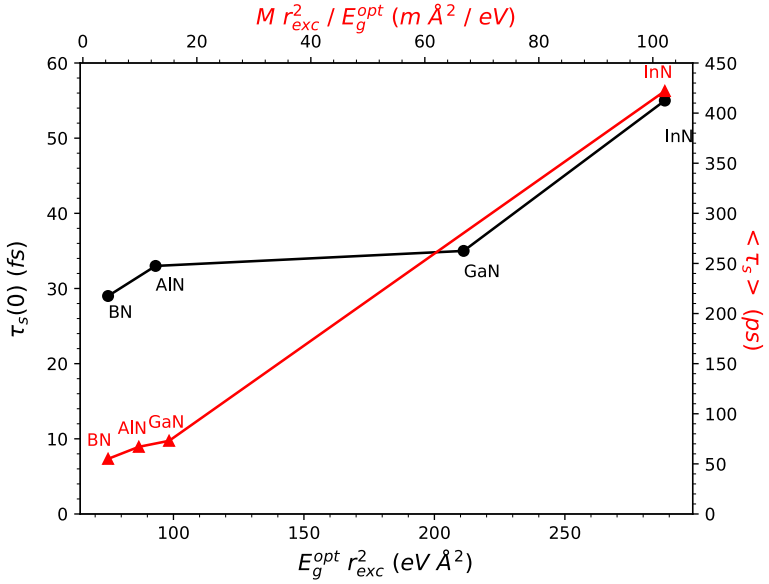

Fig. 5. Excitonic lifetimes $\tau_S(0)$ and $\langle \tau_S \rangle$ at 300 K of the 2D nitrides versus characteristic exciton parameters.

been also investigated in a variational framework by applying static sheet polarizabilities to describe the screening and the effective mass approximation. Ab-initio and model excitonic parameters are compared. We have demonstrated a significant influence of the electron-hole interactions on the optical spectra of the 2D nitrides, in particular on the absorption spectra. Strong bound exciton peaks appear below the direct quasiparticle gap. The lowest energy excitons exhibit huge exciton binding energies of 0.6–2.0 eV going from InN to BN. Thereby, the average electron-hole distances vary between 3.8 and 15.5 Å from BN to InN, indicating a transition from a Frenkel-like to a Wannier–Mott-like behavior along the row BN, AlN, GaN, and InN.

The emission properties of the 2D nitrides are illustrated by the radiative lifetimes of the lowest-energy excitons. We observed lifetimes of the order of 30–60 fs, much faster than for other 2D semiconductors. In the case of the thermal average of the excitons with finite translation vector, the radiative lifetimes increase substantially. Their low values indicate that group-III nitride sheets appear to be promising materials for active optoelectronic applications in the visible up to the vacuum ultraviolet region.

Received: 21 December 2019; Accepted: 2 April 2020
Published online: 01 July 2020

References

1. Wang, Q. H., Kalantar-Zadeh, K., Kis, A., Coleman, J. N. & Strano, M. S. Electronics and optoelectronics of two-dimensional transition metal dichalcogenides. *Nat. Nano* **7**, 699–712. https://doi.org/10.1038/nnano.2012.193 (2012).
2. Balendhran, S., Walia, S., Nili, H., Sriram, S. & Bhaskaran, M. Elemental analogues of graphene: Silicene, germanene, stanene, and phosphorene. *Small* **11**, 640–652. https://doi.org/10.1002/smll.201402041 (2015).
3. Xia, F., Wang, H., Xiao, D., Dubey, M. & Ramasubramaniam, A. Two-dimensional material nanophotonics. *Nat. Photon.* **8**, 899. https://doi.org/10.1038/nphoton.2014.271 (2014).
4. Grazianetti, C. *et al.* Optical conductivity of two-dimensional silicon: Evidence of dirac electrodynamics. *Nano Lett.* **18**, 7124–7132 (2018).
5. Nakamura, S. Nobel lecture: Background story of the invention of efficient blue ingan light emitting diodes. *Rev. Mod. Phys.* **87**, 1139–1151. https://doi.org/10.1103/RevModPhys.87.1139 (2015).
6. Nagashima, A., Tejima, N., Gamou, Y., Kawai, T. & Oshima, C. Electronic structure of monolayer hexagonal boron nitride physisorbed on metal surfaces. *Phys. Rev. Lett.* **75**, 3918 (1995).
7. Tsipas, P. *et al.* Evidence for graphite-like hexagonal AlN nanosheets epitaxially grown on single crystal ag (111). *Appl. Phys. Lett.* **103**, 251605 (2013).
8. Alamé, S. *et al.* Preparation and structure of ultra-thin GaN (0001) layers on in0. 11ga0. 89n-single quantum wells. *Mater. Sci. Semicond. Process.* **55**, 7–11 (2016).
9. Wang, P. *et al.* Experimental evidence of large bandgap energy in atomically thin AlN. *Adv. Funct. Mater.* **29**, 1902608 (2019).
10. Al Balushi, Z. Y. *et al.* Two-dimensional gallium nitride realized via graphene encapsulation. *Nat. Mater.* **15**, 1166 (2016).
11. Kecik, D. *et al.* Fundamentals, progress, and future directions of nitride-based semiconductors and their composites in two-dimensional limit: A first-principles perspective to recent synthesis. *Appl. Phys. Rev.* **5**, 011105https://aip.scitation.org/doi/abs/10.1063/1.4990377. https://doi.org/10.1063/1.4990377.(2018).
12. Zhuang, H. L., Singh, A. K. & Hennig, R. G. Computational discovery of single-layer III–V materials. *Phys. Rev. B* **87**, 165415 (2013).
13. Sahin, H. *et al.* Monolayer honeycomb structures of group-IV elements and III–V binary compounds: First-principles calculations. *Phys. Rev. B* **80**, 155453. https://doi.org/10.1103/PhysRevB.80.155453 (2009).
14. Onen, A., Kecik, D., Durgun, E. & Ciraci, S. Gan: From three- to two-dimensional single-layer crystal and its multilayer van der waals solids. *Phys. Rev. B* **93**, 085431. https://doi.org/10.1103/PhysRevB.93.085431 (2016).
15. Peng, B. *et al.* Room-temperature bound exciton with long lifetime in monolayer GaN. *ACS Photon.* **5**, 4081–4088 (2018).

16. Shu, H., Niu, X., Ding, X. & Wang, Y. Effects of strain and surface modification on stability, electronic and optical properties of GaN monolayer. *Appl. Surf. Sci.* **479**, 475–481 (2019). http://www.sciencedirect.com/science/article/pii/S0169433219305136.
17. Bacaksiz, C. *et al.* Hexagonal AlN: Dimensional-crossover-driven band-gap transition. *Phys. Rev. B* **91**, 085430 (2015).
18. Guilhon, I. *et al.* Out-of-plane excitons in two-dimensional crystals. *Phys. Rev. B* **99**, 161201(R) (2019).
19. Prete, M. S., Mosca Conte, A., Gori, P., Bechstedt, F. & Pulci, O. Tunable electronic properties of two-dimensional nitrides for light harvesting heterostructures. *Appl. Phys. Lett.* **110**, 012103 (2017).
20. Wang, V., Wu, Z. Q., Kawazoe, Y. & Geng, W. T. *J. Phys. Chem. C* **122**, 6930–6942. https://doi.org/10.1021/acs.jpcc.7b12401 (2018).
21. Sanders, N., Bayerl, D., Shi, G., Mengle, K. A. & Kioupakis, E. Electronic and optical properties of two-dimensional GaN from first-principles. *Nano Lett.* **17**, 7345–7349 (2017).
22. Liang, D. *et al.* Electronic and excitonic properties of two-dimensional and bulk InN crystals. *RSC Adv.* **7**, 42455–42461. https://doi.org/10.1039/C7RA07640A (2017).
23. Prete, M. S., Pulci, O. & Bechstedt, F. Strong in- and out-of-plane excitons in two-dimensional InN nanosheets. *Phys. Rev. B* **98**, 235431. https://doi.org/10.1103/PhysRevB.98.235431 (2018).
24. Wirtz, L., Marini, A. & Rubio, A. Excitons in boron nitride nanotubes: Dimensionality effects. *Phys. Rev. Lett.* **96**, 126104 (2006).
25. Kohn, W. & Sham, L. J. Self-consistent equations including exchange and correlation effects. *Phys. Rev.* **140**, A1133 (1965).
26. Giannozzi, P. *et al.* Quantum espresso: A modular and open-source software project for quantum simulations of materials. *J. Phys. Condens. Matter* **21**, 395502 (2009).
27. Giannozzi, P. *et al.* Advanced capabilities for materials modelling with quantum espresso. *J. Phys. Condens. Matter* **29**, 465901 (2017).
28. *Codes for GW calculation developed within the ETSF network*. https://www.etsf.eu.
29. Bechstedt, F. *Many-Body Approach to Electronic Excitations* (Springer, New York, 2016).
30. Lucia, R., Valerio, O., Francesco, S., Stefan, A. & Giovanni, O. *EXC is an exciton code working in reciprocal space, frequency domain, and using plane waves basis*. http://etsf.polytechnique.fr/exc.
31. Marsili M, Mosconi E, De Angelis F, Umari P. Large-scale *GW*-BSE calculations with N^3 scaling: Excitonic effects in dye-sensitized solar cells. Phys. Rev. B **95**(7), 075415 (2017).
32. Cudazzo, P., Tokatly, I. V. & Rubio, A. Dielectric screening in two-dimensional insulators: Implications for excitonic and impurity states in graphane. *Phys. Rev. B* **84**, 085406 (2011).
33. Pulci, O. *et al.* Excitons in two-dimensional sheets with honeycomb symmetry. *Phys. Status Solidi (b)* **252**, 72–77 (2015).
34. Keldysh, L. Coulomb interaction in thin semiconductor and semimetal films. *JETP Lett.* **29**, 658 (1979).
35. Rytova, N. S. Screened potential of a point charge in a thin film. *Mosc. Univ. Phys. Bull.* **3**, 30 (1967).
36. Matthes, L., Pulci, O. & Bechstedt, F. Influence of out-of-plane response on optical properties of two-dimensional materials: First principles approach. *Phys. Rev. B* **94**, 205408 (2016).
37. Moody, G., Schaibley, J. & Xu, X. Exciton dynamics in monolayer transition metal dichalcogenides. *JOSA B* **33**, C39–C49 (2016).
38. Palummo, M., Bernardi, M. & Grossman, J. C. Exciton radiative lifetimes in two-dimensional transition metal dichalcogenides. *Nano Lett.* **15**, 2794–2800 (2015).
39. Cahangirov, S., Topsakal, M., Aktürk, E., Şahin, H. & Ciraci, S. Two-and one-dimensional honeycomb structures of silicon and germanium. *Phys. Rev. Lett.* **102**, 236804 (2009).
40. Bayerl, D. *et al.* Deep ultraviolet emission from ultra-thin GaN/AlN heterostructures. *Appl. Phys. Lett.* **109**, 241102 (2016).
41. de Carvalho, L. C., Schleife, A. & Bechstedt, F. Influence of exchange and correlation on structural and electronic properties of AlN, GaN, and InN polytypes. *Phys. Rev. B* **84**, 195105. https://doi.org/10.1103/PhysRevB.84.195105 (2011).
42. Marinopoulos, A. *et al.* Optical absorption and electron energy loss spectra of carbon and boron nitride nanotubes: A first-principles approach. *Appl. Phys. A* **78**, 1157–1167 (2004).
43. Berseneva, N., Gulans, A., Krasheninnikov, A. V. & Nieminen, R. M. Electronic structure of boron nitride sheets doped with carbon from first-principles calculations. *Phys. Rev. B* **87**, 035404. https://doi.org/10.1103/PhysRevB.87.035404 (2013).
44. Bacaksiz, C., Dominguez, A., Rubio, A., Senger, R. T. & Sahin, H. H-aln-Mg (oh) 2 van der waals bilayer heterostructure: Tuning the excitonic characteristics. *Phys. Rev. B* **95**, 075423 (2017).
45. Pulci, O. *et al.* Strong excitons in novel two-dimensional crystals: Silicane and germanane. *EPL (Europhys. Lett.)* **98**, 37004 (2012). http://stacks.iop.org/0295-5075/98/i=3/a=37004.
46. Gori, P., Pulci, O., Marsili, M. & Bechstedt, F. Side-dependent electron escape from graphene- and graphane-like sic layers. *Appl. Phys. Lett.* **100**, 043110. http://link.aip.org/link/?APL/100/043110/1. https://doi.org/10.1063/1.3679175 (2012).
47. Dmitriev, A. & Oruzheinikov, A. The rate of radiative recombination in the nitride semiconductors and alloys. *J. Appl. Phys.* **86**, 3241–3246 (1999).
48. Jhalani, V. A., Chen, H.-Y., Palummo, M. & Bernardi, M. First-principles exciton radiative lifetimes in wurtzite GaN. arXiv preprint arXiv:1908.09962 (2019).
49. Kokalj, A. Xcrysden–a new program for displaying crystalline structures and electron densities. *J. Mol. Graph. Model.* **17**, 176–179 (1999).

Acknowledgements

O.P. and I.K. acknowledge financial support from the EU MSCA HORIZON2020 projects 'CoExAN' (GA644076) and DiSeTCom (GA 823728). F.B. acknowledges travel support by INFN Tor Vergata. We thank Prof. Maurizia Palummo for useful discussions.

Author contributions

M.S.P., D.G., O.P. and I.K. performed the calculations. F.B., V.O. and O.P. conceived the project. All authors wrote the paper. All authors analyzed the results. All authors reviewed the manuscript.

Competing interests

The authors declare no competing interests.

Additional information

Supplementary information is available for this paper at https://doi.org/10.1038/s41598-020-67667-2.

Correspondence and requests for materials should be addressed to D.G.

Reprints and permissions information is available at www.nature.com/reprints.

Publisher's note Springer Nature remains neutral with regard to jurisdictional claims in published maps and institutional affiliations.